PFC/JA-87-13

The Cusp Map In The Complex-Frequency Plane For Absolute Instabilities

K. Kupfer, A. Bers and
A. K. Ram

March 1987

Research Laboratory of Electronics

and

Plasma Fusion Center

Massachusetts Institute of Technology

Cambridge, MA 02139

This work was supported by NSF Grant No. ECS-8515032 and by DOE Contract No. DE-AC02-78ET-51013.

Submitted for publication to The Physics of Fluids

THE CUSP MAP IN THE COMPLEX-FREQUENCY PLANE FOR ABSOLUTE INSTABILITIES

by

K. Kupfer, A. Bers, and A. K. Ram

Research Laboratory of Electronics,

and

Plasma Fusion Center

Massachusetts Institute of Technology

Cambridge, MA 02139

PACS numbers: 03.40.-t, 03.40.Gc, 47.20.Ft

Abstract

It is well known that absolute instabilities can be located by prescribed mappings from the complex frequency plane to the wave-number plane through the dispersion relation $D(\omega, k) = 0$. However, in many systems of physical interest the dispersion relation is polynominal in ω while transcendental in k, and the implementation of this mapping procedure is particularly difficult. If one maps consecutive deformations of the Fourier integral path (originally along the real k-axis) into the ω-plane, points having $(\partial D/\partial k) = 0$ are readily detected by the distinctive feature of their local maps. It is shown that a simple topological relationship between these points and the image of the real k-axis determines the stability characteristics of the system, without mapping from the ω-plane back into the k-plane.

I. INTRODUCTION

The space-time evolution of a linear instability is described by the Green's function defined as

$$G(x,t) = \int_L \frac{d\omega}{2\pi} \int_F \frac{dk}{2\pi} e^{i(kx-\omega t)} D^{-1}(\omega,k) \tag{1}$$

for one-dimensional perturbations whose frequency, ω, and wavenumber, k, are related by the dispersion relation, $D(\omega,k) = 0$. The unstable Green's function can evolve in two distinctly different ways: it can encompass the origin of excitation, in which case at any fixed point in space the disturbance grows without bound, or it can grow and propagate away from the origin so that $G(x, t \to \infty) = 0$ at any given finite x. In most cases the Fourier-Laplace integral in Eq.(1) cannot be evaluated for all t. However, for a general dispersion relation one may obtain the time-asymptotic Green's function by a well known method of analytic continuation in which the Laplace contour (L) is deformed towards the lower half of the complex ω-plane.[1]

The procedure is shown skematically in Fig. 1. First, the domain of absolute convergence (DAC) of $D^{-1}(\omega,k)$ is defined for real k by mapping the Fourier contour (F) into the ω-plane through the dispersion relation. The DAC in ω is everywhere above the highest branch of this mapping. As the L-contour, originally in the DAC, is deformed towards the lower half ω-plane, its image in the k plane will cross the original F-contour along the real k-axis. To maintain causality, the F-contour must be deformed off the real k-axis in such a way as to avoid the crossing. This process of consecutive contour deformations can be continued until two branches in the mapping of the deformed L-contour, originally from opposite sides of F, "pinch" the deformed F-contour at a saddle-point in the k-plane. Such saddle-points are called "pinch-points", distinguishing them from the general class of multiple roots in the mapping of a given ω through $D(\omega,k) = 0$. If the corresponding branch-point in the ω-plane has a positive imaginary component it will dominate the time asymptotic response and $G(x, t \to \infty)$ can be approximated by a simple integral around the branch cut. This is the case for an absolute instability. On the other hand, if L can be deformed to the real ω-axis, the instability is convective.

A unified treatment of both instability types is obtained by considering the Green's function at the origin of a reference frame moving with nonrelativistic velocity V[2], so

that

$$G(Vt,t) = \int_L \frac{d\omega'}{2\pi} \int_F \frac{dk}{2\pi} e^{-i\omega' t} D_V^{-1}(\omega', k) \tag{2}$$

where $\omega' = \omega - kV$ is the Doppler shifted frequency and $D_V(\omega', k) = D(\omega' + kV, k)$. The above described mappings through $D_V(\omega', k) = 0$ will possess pinch-points, for some range of observer velocities, one of which has the largest temporal growth rate, ω'_{0i}, for a given V. By varying the observer velocity one obtains the function ω'_{0i}(V), which is the asymptotic pulse since $ln|G(Vt,t)| = \omega'_{0i}(V)t$ and $x = Vt$. The edges of the pulse are given by $V = V_\pm$ where $\omega'_{0i}(V_\pm) = 0$; if the edge velocities, $V_\pm$, are of the same sign then the instability is convective, otherwise it is absolute.

We see that the space-time evolution of a linear instability is characterized by the so called "pinch-points" which are located in a process of analytic continuation where L is deformed towards the lower half ω-plane. As formulated, this process depends on solving the dispersion relation for k as a function of ω. However, in many physical problems the dispersion relation is a transcendental function of k while only a polynominal function of ω. This is often the case when a medium supports perturbations whose corresponding eigenfunctions are spatially bounded in one direction and the dispersion relation is obtained by solving a particular eigenvalue problem. In such cases it seems unfortunate that the procedure which locates pinch-points depends on solving the dispersion relation for k as a function of ω, since the computation of ω as a function of k is much easier.

In this paper we will develop a procedure which identifies pinch-points by mappings only from the k-plane into the ω-plane. This has been attempted by previous authors. Fainberg et.al. [3] formulated a criterion for absolute instability which depended only on the image of the real k-axis in the ω-plane and the subsequent position of the highest branch-point beneath this image. When the "pinch-point" technique, summarized above, was developed, Briggs [4] compared it with the method of Fainberg, which he showed to be insufficient. Later, Derfler [5] supplemented Fainberg's criterion by mappings from the k-plane only. Recently, however, in an attempt to implement Derfler's technique, we found it to be unreliable. This lead us to develop the criterion which is proved rigoursly in Section II. In Section III, the pinch-points of two mathematical dispersion relations are found by mapping the appropriate contours from the k-plane into the ω-plane and the

latter example is shown to be a case for which Derfler's criteria fail. We will conclude with a recent example from hydrodynamics [6] in which our technique is valuable.

II. THE MAPPING PROCEDURE

The instability is first examined by mapping the F-contour into the ω-plane. Since the mapping of a given k into the ω-plane is generally multi-valued, the various images of the F-contour will be called $\omega_{F\alpha}$, where α is a positive integer. Consider the case when the mapping reveals only one unstable branch, this branch shall be called ω_F and the subscript α will be dropped (as in Fig. 1). The inverse mapping of ω_F into the k-plane will generate a set of n contours, $k_\beta(\omega_F)$ with $\beta = 1, 2, ...n$, where n is the order of the dispersion relation in k, which goes to infinity when the functional dependence on k is transcendental. There is always a unique contour in the set $k_\beta(\omega_F)$ which corresponds to F, as shown in Fig. 2. The mapping of a given ω into the k-plane may be rendered single-valued by constructing a multi-sheeted ω-plane with n Riemann sheets. The contour ω_F is actually a set of n contours in the multi-sheeted ω-plane, each corresponding to a single contour in the set $k_\beta(\omega_F)$. Hence there is a unique contour, $\tilde{\omega}_F$, which is defined in the multi-sheeted ω-plane and maps only onto F. Similarly, if there are two unstable branches, ω_{F1} and ω_{F2}, then there are two contours in the multi-sheeted ω-plane, $\tilde{\omega}_{F1}$ and $\tilde{\omega}_{F2}$, which map only onto F.

Simultaneous solutions of $D(\omega, k) = 0$ and $\partial D(\omega, k)/\partial k = 0$ are branch-points in the ω-plane. In particular, a given $\omega = \omega_0$, which satisfies $D(\omega_0, k) = \partial D(\omega_0, k)/\partial k = 0$ for a specific value of $k = k_0$, where $\partial^2 D(\omega_0, k)/\partial k^2 \neq 0$, has only n-1 distinct images in the k-plane, so that the point $\omega = \omega_0$ corresponding to $k = k_0$ connects two sheets of the multi-sheeted ω-plane. On each of these two sheets consider a vertical ray, R_1 and R_2 respectively, which connects an ω on L to the branch-point at $\omega = \omega_0$ (as in Figures 3, 4, and 5). The images of R_1 and R_2 in the k-plane merge at the point $k = k_0$. For the branch-point at $\omega = \omega_0$ to correspond to a pinch-point, it is necessary and sufficient that the k-plane images of R_1 and R_2 start on opposite sides of F. This is simply a re-statement of the original criteria shown skematically in (Fig.2) and its implementation still requires mapping from the ω-plane into the k-plane. On the other hand, it follows that if the images of R_1 and R_2 start on opposite sides of F and merge at a single point (not on F),

then one, or perhaps both, of these images must cross F. Furthermore, the total combined number of crossings made by both images must be odd. Since only the contours $\tilde{\omega}_{F\alpha}$ map onto F, the image of R_1 crosses F in the k-plane only when R_1 crosses one of the contours $\tilde{\omega}_{F\alpha}$ in the ω-plane. The same is true for R_2. Therefore, one may count the number of times each of the vertical rays, R_1 and R_2, crosses each of the contours $\tilde{\omega}_{F\alpha}$; only when the total combined number of crossings is odd does the branch-point at $\omega = \omega_0$ correspond to a pinch-point. Furthermore, the same must hold true for a higher-order branch-point (one for which $\partial^2 D(\omega, k)/\partial k^2$ also vanishes) if the connected Riemann sheets are considered in pairs [7].

Application of this criterion to the simple proto-type shown in Fig. 3a, reveals that branch-points covered only once by $\tilde{\omega}_F$ always correspond to pinch-points. Topologically identical cases were studied by Fainberg [3] and the same result was concluded. On the other hand, a branch-point located beneath two contours, $\tilde{\omega}_{F1}$ and $\tilde{\omega}_{F2}$ (as in Fig. 4), does not correspond to a pinch-point, since R_1 crosses each contour once, while R_2 makes no crossings. An example of this type was studied by Briggs [4] to show that the various branches of the mapping of a given k into the ω-plane cannot always be handled separately, as stated by Fainberg. We point out in addition that an example can be constructed where there is only one branch, yet Fainberg's technique still fails. Consider a contour $\tilde{\omega}_F$ which loops around a single branch-point from above, as shown in Fig. 5. Each of the rays, R_1 and R_2, crosses $\tilde{\omega}_F$ once, so that the combined number of crossings is even. Therefore the enclosed branch-point does not correspond to a pinch-point and does not contribute to the asymptotic response, even though it lies in the upper-half plane beneath $\tilde{\omega}_F$, as considered sufficient by Fainberg. Derfler [5] supplemented Fainberg's criterion by assuming that if $k = k_o$ is a pinch-point, then the vertical line passing through k_o, when mapped into the ω-plane, must start and end on different Riemann sheets. However, numerous counter examples can be constructed for which Derfler's assertion is invalid. In particular, his criteria fail for examples of the type shown in Fig. 5 [8]. Our criterion, which is completely general, may be used, together with the following procedure, to determine the stability characteristics of any dispersion relation.

The procedure requires one to map a section of the k-plane into a specified region (S)

located beneath $\tilde{\omega}_F$ (Fig.6). The image of S in the k-plane is bounded on one side by the F-contour. A set of vertical rays along the range of unstable wave-numbers is mapped into the ω-plane. Each ray is terminated as its image leaves the specified region (Fig. 6b). These rays, originally parallel in the k-plane, may have images which intersect, thus indicating a branch-point somewhere in S. The singularity is identified by the angle-doubling property of its local map, i.e. $(\omega - \omega_0) \sim (k - k_0)^2$. This is the case in Fig. 6b, which shows the branch-point nested at the edge of a typical "cusp"-like trajectory. If a branch-cut is taken downward from the singularity one obtains a mapping consistent with the multi-sheeted structure implied by the contour $\tilde{\omega}_F$ (Fig. 6c). In this case the branch-point is covered only once by $\tilde{\omega}_F$ and thus corresponds to a pinch-point. Of course, the same technique works for higher order branch-points, the only difference is in the local map, characterized by the first non-vanishing derivative of ω as a function of k. In many problems it is simpler to replace the vertical rays shown in Fig. 6a with a set of horizontal contours that represent deformations of the Fourier integral path (Fig. 7a). In the ω-plane, these contours will progress downward from $\tilde{\omega}_F$ and form a cusp as they approach the singularity (Fig. 7b). Once again the branch-point is located by the angle-doubling (tripling, etc.) property of its local map. Finally, this same procedure can be systematically generalized for dispersion relations with multiple unstable branches. The subtleties of the analysis are displayed in the second example considered in the next section.

III. TWO MATHEMATICAL EXAMPLES

Consider the simple dispersion relation,

$$D(\omega, k) = \omega - [\frac{1}{3}(k - i)^3 + i - kV] \tag{3}$$

which has a parametric dependence on V. For all V, the range of unstable wave-numbers is $-2/\sqrt{3} < k_r < 2/\sqrt{3}$, with a maximum growth rate of $\omega_i = 4/3$ at $k_r = \omega_r = 0$. The branch-points can easily be found by setting $d\omega/dk = 0$, which gives

$$k_\pm = i \pm \sqrt{V} \tag{4a}$$

$$\omega_\pm = (1 - V)i \pm \sqrt{V}(\frac{-2V}{3}) \tag{4b}$$

Now applying the technique developed in section II we will map the F contour into the ω-plane for V=1. A set of lines parallel to F with increasing k_i will have images in the ω-plane as shown in Fig. 8a. The images form cusps at $\omega = \pm 2/3$, which corresponds to the values given by equation (4b) with V=1. Both singularities are covered once by $\tilde{\omega}_F$ so that each corresponds to a pinch-point. As V decreases from unity these branch-points move into the upper half ω-plane and their separation along the real ω-axis decreases, so that for an arbitrary value of $0 < V < 1$ the picture remains qualitatively similar to the case when V = 1. However, when V = 0 the two branch-points merge at $\omega = i$ and as V becomes slightly negative only the lower branch-point remains beneath $\tilde{\omega}_F$ (Fig. 8b); the upper branch point slips out onto the third Riemann sheet where it no longer corresponds to a pinch-point. As V decreases further the branch-point beneath $\tilde{\omega}_F$ moves upward until at V = -1 it moves onto $\tilde{\omega}_F$ at $\omega = (4/3)i$, thus attaining the maximum growth rate. As V decreases below -1, the singularity moves downward in the ω-plane and remains beneath $\tilde{\omega}_F$ (Fig. 8c). Finally, we see that the temporal growth rate associated with the pinch-point is given for all V by the imaginary part of ω_- in Eq. (4b), so that if V were the observer velocity, then Fig. 9 would be the pulse shape.

We now consider a more complex example that will show off some of the subtleties involved in the analysis. The dispersion relation has the form encountered in coupled mode problems

$$D(\omega, k) = [\omega - \omega_1(k)][\omega - \omega_2(k)] - \gamma \tag{5a}$$

where we let

$$\omega_1(k) = k + 3i \tag{5b}$$

$$\omega_2(k) = 2i - 2k - ik^2 \tag{5c}$$

and γ is a coupling parameter. Notice that general analytic expressions can no longer be obtained for the branch-points, since the result of setting $D(\omega, k) = \partial D(\omega, k)/\partial k = 0$ is a fifth order equation in k. Here we obtain results for $\gamma = 0.1$. The mapping of F into the ω-plane yields two branches, ω_{F1} and ω_{F2}, where ω_{F1} is the highest (Fig. 10a). If the F-contour is deformed into the lower half k-plane one of its two images will progress

downward from ω_{F1} while the other progresses upward from ω_{F2}. In particular, a set of k-plane contours with k_i=constant < 0 is mapped into the ω-plane resulting in Fig. 10b. We see that the images progressing downward from ω_{F1} form a saddle-map with those progressing upward from ω_{F2}. For values of $k_i < -0.1$ the images move towards opposite sides of the ω_i-axis forming cusps at $\omega = (2.7i \pm .3)$. Furthermore, since ω_{F1} in Fig. 10b may be placed on a single Riemann sheet and identified as $\tilde{\omega}_{F1}$, both branch-points located beneath it correspond to pinch-points. Taking the branch-cut between the two singularities results in the multi-sheeted diagram shown in Fig. 10c. Also shown in Fig. 10c is a third branch-point which lies beneath $\tilde{\omega}_{F2}$. This is easily found by assuming $\omega \approx \omega_2(k)$ and $d\omega_2(k)/dk = 0$. Before our criterion can be applied to the third branch point one must deform the horizontal branch cut so that it does not cover the singularity in question (Fig. 10d) [9]. The third branch-point now appears on sheet one beneath both $\tilde{\omega}_{F1}$ and $\tilde{\omega}_{F2}$; therefore it does not corresond to a pinch-point.

The contours C_1 and C_2, shown in Fig. 10e, are the images of the line $k_r = -0.08$. We see that C_1 nearly passes through the singularity at $\omega = (2.7i - 0.3)$; in fact, it loops around the branch-point passing from sheet one onto sheet two and then back onto sheet one (see Fig. 10c). Even though C_1 starts and ends on the same Riemann sheet, the enclosed branch-point corresponds to a pinch-point, thus violating Derfler's criteria [5].

IV. A PHYSICAL EXAMPLE

It is well known that vortices are observed in the wake of fluid flowing past a long cylinder. Flows with Reynolds numbers greater than about forty generate a staggered array of vortices known as the von Karman vortex street. Vortices are formed at a specific frequency and are separated by a unique distance. Flows with Reynolds numbers smaller than forty are observed to produce vortices only when the cylinder is driven to oscillate by an external source. In this case vortices are created at the frequency of the source and are convected downstream by the flow. These phenomena have been recently explained by an absolute versus convective instability analysis of the time-averaged flow in the wake [6].

The local dispersion relation for waves propagating parallel to the flow is obtained by solving the inviscid Orr-Sommerfeld equation in a strip about $x = x_0$, where the unperterbed flow is described by the velocity profile $U(y, x_0)$ (Fig. 11). In particular, the

stream function of the pertubation, $\phi(y)exp[ik(x-x_0)-i\omega t]$, satisfies

$$(kU-\omega)(\frac{d^2\phi}{dy^2}-k^2\phi)-k\frac{d^2U}{dy^2}\phi=0 \tag{6}$$

where the domain of y is truncated by assuming that d^2U/dy^2 is identically zero for $y \geq y_1 \gg d$. As a result, ϕ(y) must match to a decaying exponential at y=y_1; the other boundary condition is obtained by requiring $\phi(y)$ to be either symmetric or anti-symmetric. Equation (6) can now be solved on the domain $0 \leq y \leq y_1$ using a finite difference scheme which results in a matrix eigenvalue problem of the form

$$\omega B_{\alpha\beta}(k)\phi_\beta = A_{\alpha\beta}(k)\phi_\beta \tag{7}$$

where the matrix elements are functions of k. Furthermore, the functional dependence on k is transcendental as prescribed by the boundary condition at $y = y_1$. The result is that Eq. (7) is convenient for mapping a given k into the complex ω-plane, but cannot readily be inverted for k as a function of ω.

Measurements of the average flow for a given Reynolds number, Re, allow one to construct the local velocity profile, $U(y, x_o)$. Once $U(y, x_0)$ and the symmetry of $\phi(y)$ are specified, Eq.(7) provides a unique mapping from the k-plane into the ω-plane. For a variety of Re and x_0, Triantafyllou et. al. [6] find a single unstable contour, ω_F, which does not overlap itself. This contour can be placed on a single Riemann sheet of the multi-sheeted ω-plane, where it is labeled $\tilde{\omega}_F$. Deformations of the F-contour into the lower-half k-plane have images which progress downward from $\tilde{\omega}_F$ until a cusp is formed. The singularity located by this cusp corresponds to a pinch-point (as proven in Section II) and when it is in the upper half ω-plane the system is absolutely unstable. For low over-critical Reynolds numbers (Re>40), the near wake is found absolutely unstable when $\phi(y)$ is symmetric (Fig. 12a). As x_0 is increased, the singularity in the ω-plane gradually moves downward, finally going into the lower half plane for $x_0 > 3.5d$ (Fig. 12b). At the same Re, the anti-symmetric mode is also unstable, but the corresponding pinch singularity is always in the lower-half ω-plane. On the other-hand, for under-critical Reynolds numbers (Re<40) both modes lead to a convective instability, which is consistent with the observation that in this regime vortices are formed only when an external excitation of the cylinder is

provided. For over-critical Reynolds numbers the formation frequency and the vortex spacing are predicted accurately by the real parts of the frequency and wave-number of the pinch-point. Furthermore, the preferred mode characteristics predicted by the analysis are consistent with observations. Namely, the symmetric mode, which must lead to a staggered array of vortices, is time-asymptotically dominant over the anti-symmetric mode, which could only produce a non-staggered array. Thus the analysis shows that in the wake of a cylinder there is a region of absolute instability, where the vortex street is formed, followed by convectively unstable region where the vortex street propagates and maintains itself. Trintafyllou et. al. [6] also analyzed the stability of a turbulent profile at Re=140,000 and again found good agreement with the observed characteristics of the vortex formation.

ACKNOWLEDGMENT

This work was supported by NSF Grant No. ECS-8515032 and by DOE Contract No. DE-AC02-78ET-51013.

REFERENCES AND NOTES

1. A. Bers in *Handbook of Plasma Physics* (gen. eds. M.W. Rosenbluth and R.Z.Sagdeev), *Vol. 1, Basic Plasma Physics* (vol. eds. A.A.Galeev and R.N.Sudan), Chapter 3.2, North Holland Publ. Co., 1983.
2. A relativistic generalization of this has been given recently: A. Bers, A. K. Ram, and G. Francis, Phys. Rev. Letters **53**. 1457 (1984); the analysis we present can be readily applied to the relativistic case.
3. Ya.B.Fainberg, V.I.Kurilo, and V.D.Shapiro, Sov.Phys.Tech.Phys. **6**, 459 (1961)
4. R.J.Briggs, *Electron-Stream Interaction with Plasmas*, Research Monograph No. 29, Appendix A, (M.I.T. Press, Cambridge, Mass. 1964)
5. H.Derfler, Phys. Rev. A **1**, 1467 (1970).
6. G.S.Triantafyllou, M.S.Triantafyllou, and C.Chryssostomidis, J. Fluid Mech., **170**, 461 (1986).
7. In the case of a second order branch-point, for example, one must consider three vertical rays, R_1, R_2, and R_3, defined in the same way as before, one on each of the three Riemann sheets connected by the branch-point. If the combined number of crossings of the contours $\tilde{\omega}_{F\alpha}$ made by any of the combinations, R_1 and R_2, R_1 and R_3, or R_2 and R_3, is odd, then the corresponding singularity in the k-plane will pinch the deformed F-contour.
8. Consider the specific mapping

$$\omega = \frac{(k+i)^3}{3} + 0.9k + i - \frac{ik^4}{40}$$

which has three branch-points one in the upper-half ω-plane beneath $\tilde{\omega}_F$, as in Fig. 5. The image of the imaginary k-axis passes through all three branch-points, starting and ending on different Riemann sheets, so that Derfler's criteria are satisfied, yet the system does not have an absolute instability.
9. Otherwise vertical rays of the type defined in Section II (R_1 and R_2) would cross the branch-cut and accordingly their images in the k-plane would be discontinuous.

FIGURE CAPTIONS

Figure 1. Contour deformations for the time-asymptotic evaluation of the Fourier-Laplace integral; ω_F is the highest image of F in the ω-plane; $k_1(L)$ and $k_2(L)$ are two images of L in the k-plane; the images of L' pinch the deformed F-contour at the saddle-point marked $\times$; the corresponding branch-point is shown with its branch-cut taken straight down.

Figure 2. Various branches in the mapping of ω_F into the k-plane.

Figure 3. Simple topological configuration for a branch-point which corresponds to a pinch-point:

(a) The contours R_1 and R_2 are defined in the multi-sheeted ω-plane;

(b) Mapping of R_1 and R_2 into the k-plane - only the image of R_1 crosses F. Note that $k(L_1)$ corresponds to $k_1(L)$ in the notation of Fig. 1.

Figure 4. Branch-point which does not correspond to a pinch-point indicating the failure of Fainberg's criteron for the case of multiple contours $\tilde{\omega}_{F_a}$.

Figure 5. Branch-point beneath a single overlapping contour $\tilde{\omega}_F$.

Figure 6. Mappings from the k-plane into region (S) of the ω-plane bounded by $\tilde{\omega}_F$ and the dashed line.

(a) Vertical rays terminated as their images leave S; $\times$ marks a saddle-point;

(b) Corresponding images in the ω-plane; contour (5) shows typical "cusp"-like form near branch-point;

(c) Branch-cut consistent with Fig. (6b); contours 4, 5, 6, and 7 pass through the cut onto another sheet.

Figure 7. Consecutive deformations of the F-contour in an attempt to detect the pinch-point (marked $\times$):

(a) Horizontal line segments mapped into the ω-plane;

(b) Images in the ω-plane show singularity beneath $\tilde{\omega}_F$. (The dashed line is shown in connection with Fig. 6.)

Figure 8. Contours k_i = const. are mapped from the k-plane through Eq. (3) for various values of V:

(a) V = 1; A, B, and C are the consecutive images of $k_i = 0.3$, 0.6, and 0.9; segment C detects branch-points at $\omega = \pm 2/3$;

(b) $V = -0.1$; A, B, and C are the consecutive images of $k_i = 0.2$, 0.4, and 0.7;

(c) $V = -1.5$; A and B are the consecutive images of $k_i = -0.1$ and -0.22.

Figure 9. From Eq. (4b), the imaginary part of the lower branch-point as a function of V gives the asymptotic pulse shape.

Figure 10. Mappings from the k-plane through Eq. (5):

(a) Image of the F-contour in the ω-plane for $-1.5 < k_r < 1.5$;

(b) A, B, C, and are the consecutive images of $k_i = -0.1, -0.15$, and -0.3.

(c) Three-sheeted ω-plane showing the two branch- points detected in Fig. (10b) and a third which lies beneath $\tilde{\omega}_{F2}$. C_1 and C_2 are the two images of $k_r = -0.08$, showing the failure of Derfler's criteria. (The drawings are not to scale.)

(d) Deformation of horizontal branch-cut shows that the lower branch-point in Fig. 10c does not correspond to a pinch-point.

(e) For the test of Derfler's criteria, C_1 and C_2 are the images of $k_r = -0.08$.

Figure 11. Average flow in the wake of a cylinder: U_o is the incident flow, $U(y, x_o)$ is the profile at $x = x_o$.

Figure 12. Parallel deformations of the F-contour mapped into the ω-plane for flow at a Reynolds number of 56; contours A through D are the consecutive images of $k_i = -0.50$, -0.75, -1.0, and -1.1. In (a) the profile is taken at a distance of two diameters behind the cylinder, while in (b) the distance is 3.5 diameters. (The wave-number and frequency are normalized to d and d/U_o, respectively.) [6]

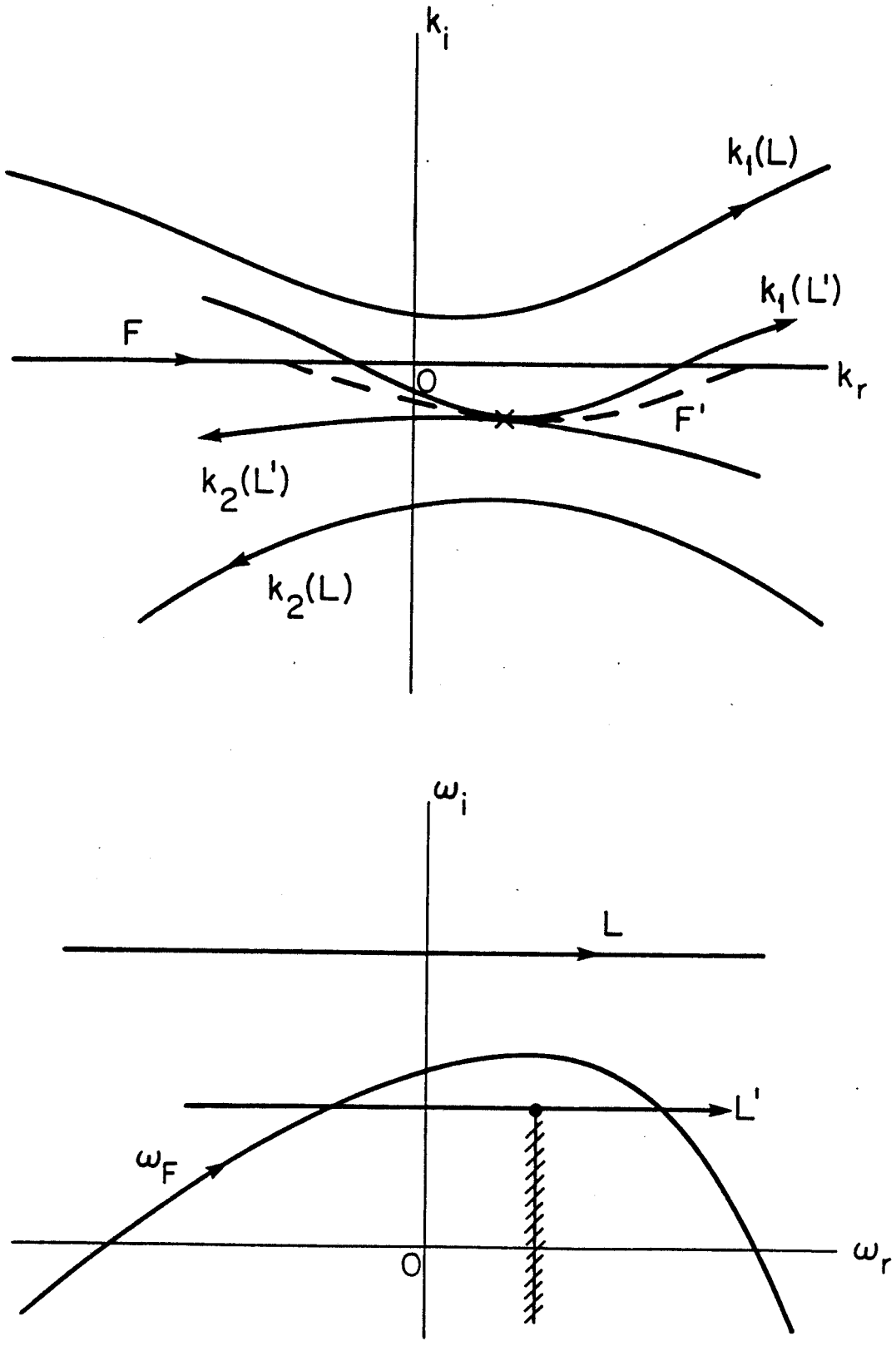

Figure 1

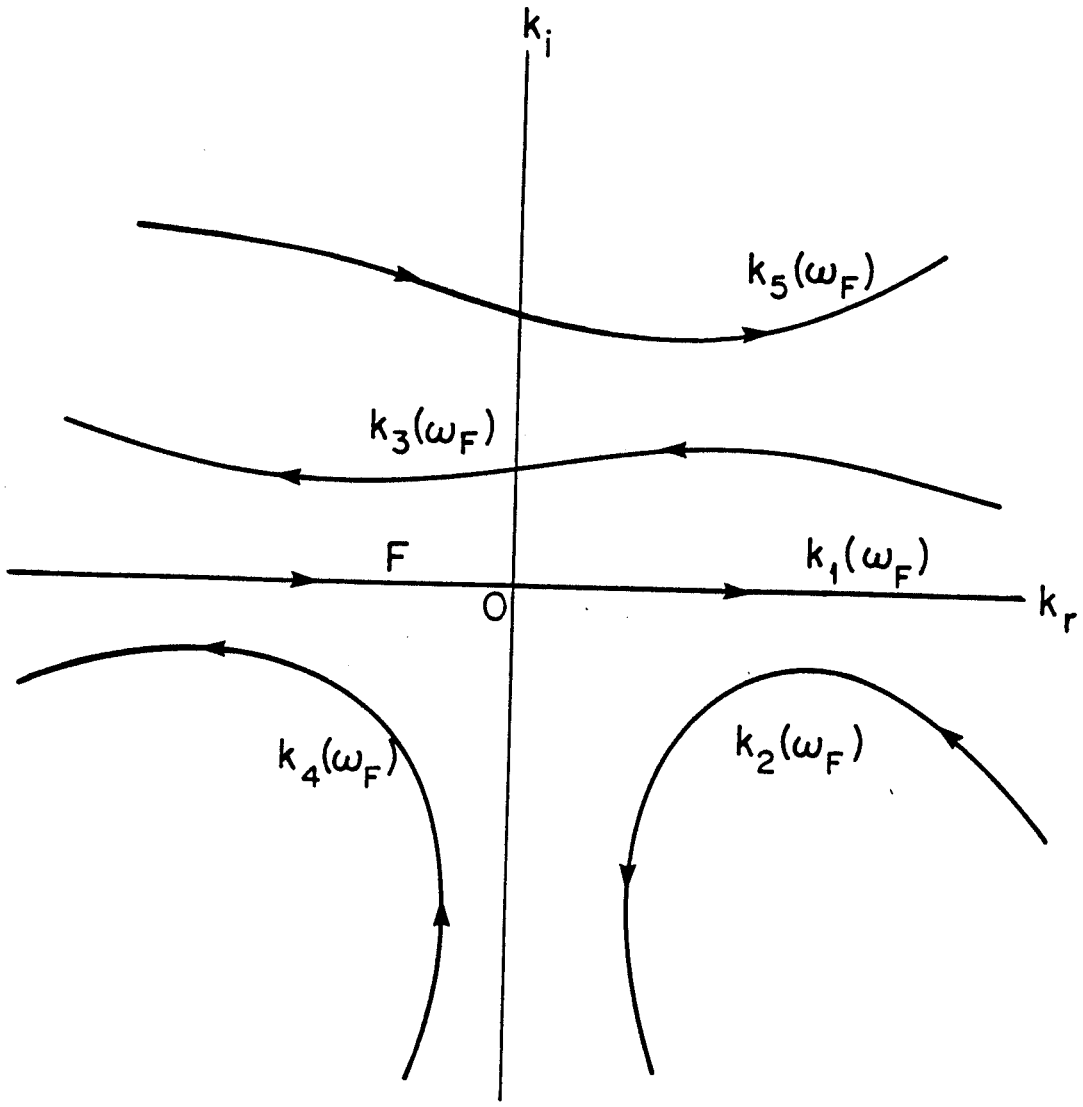

Figure 2

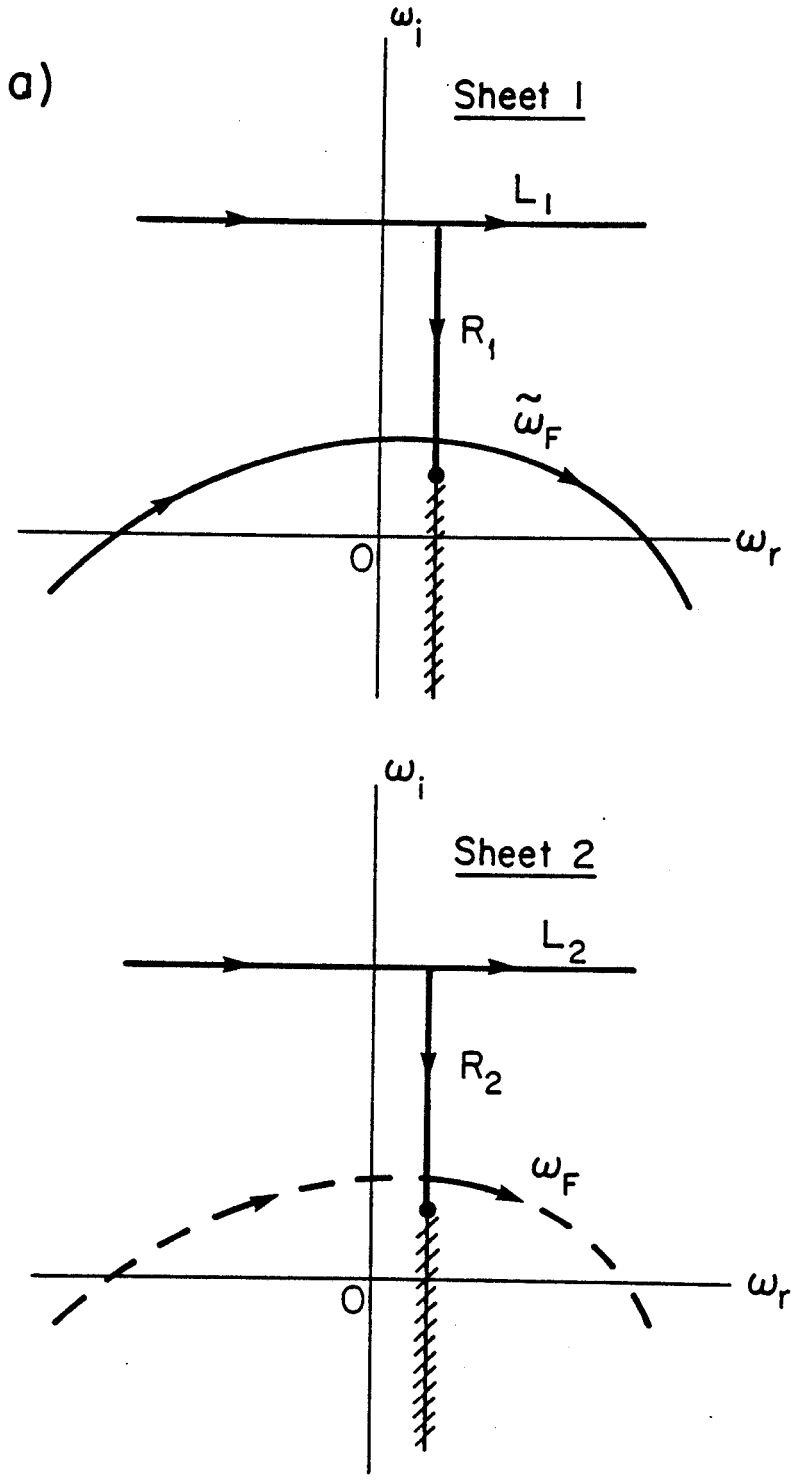
a)
ω_i
Sheet 1
L_1
R_1
$\tilde{\omega}_F$
O
ω_r
ω_i
Sheet 2
L_2
R_2
ω_F
O
ω_r

Figure 3a

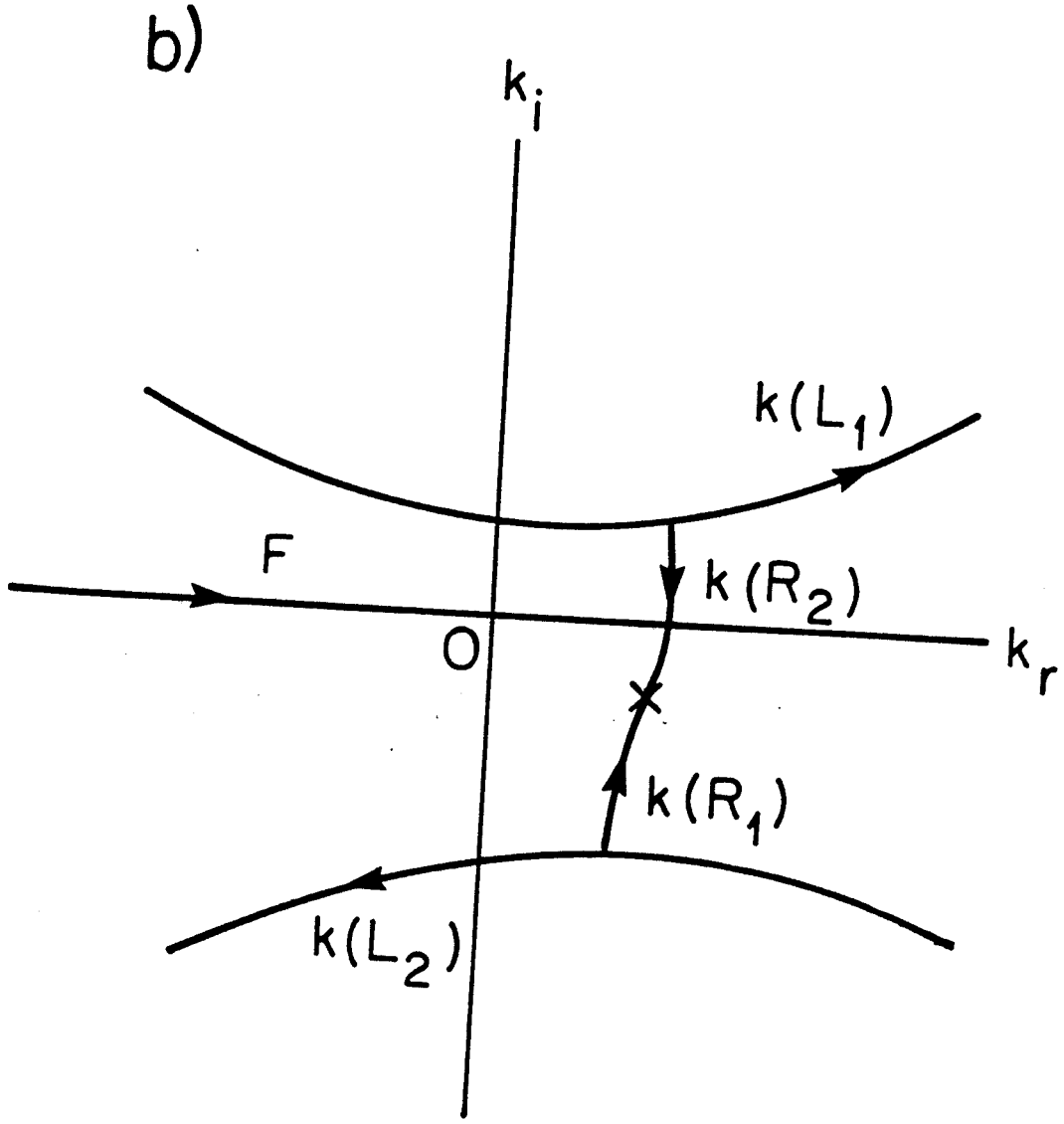

Figure 3 b

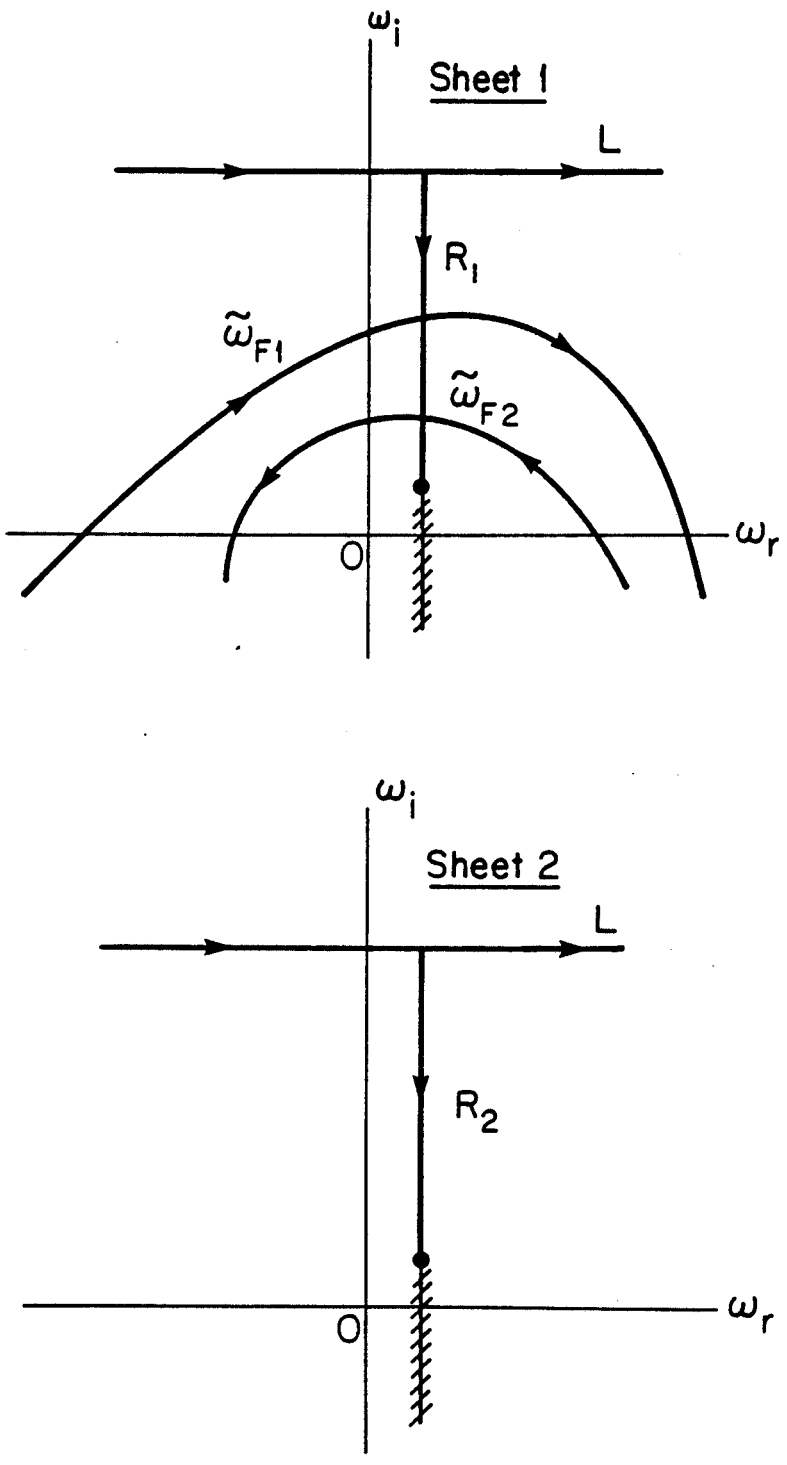
ω_i
Sheet 1
L
R_1
$\tilde{\omega}_{F1}$
$\tilde{\omega}_{F2}$
O
ω_r
ω_i
Sheet 2
L
R_2
O
ω_r

Figure 4

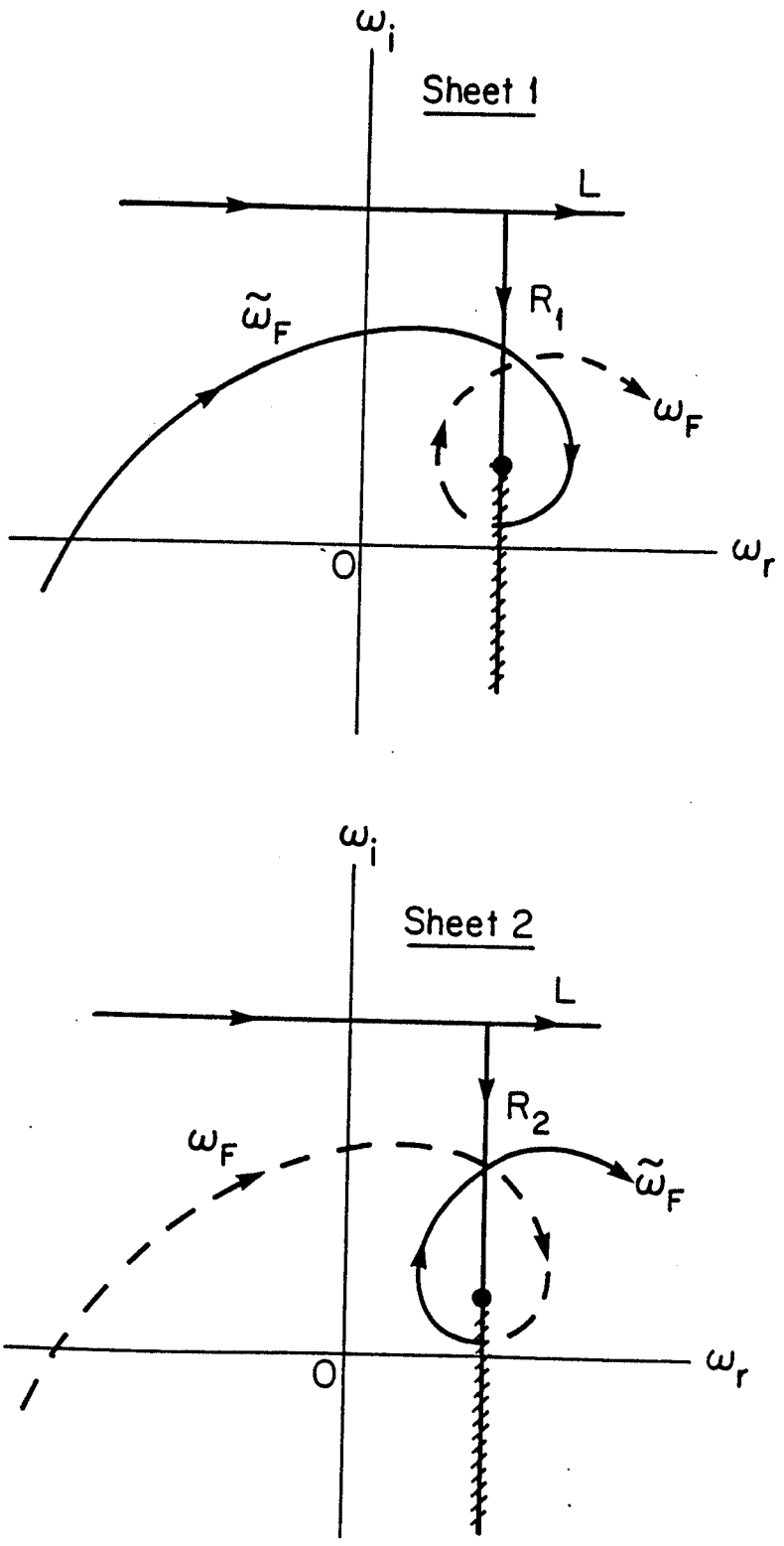
ω_i
Sheet 1
L
R_1
$\tilde{\omega}_F$
ω_F
O
ω_r
ω_i
Sheet 2
L
R_2
ω_F
$\tilde{\omega}_F$
O
ω_r

Figure 5

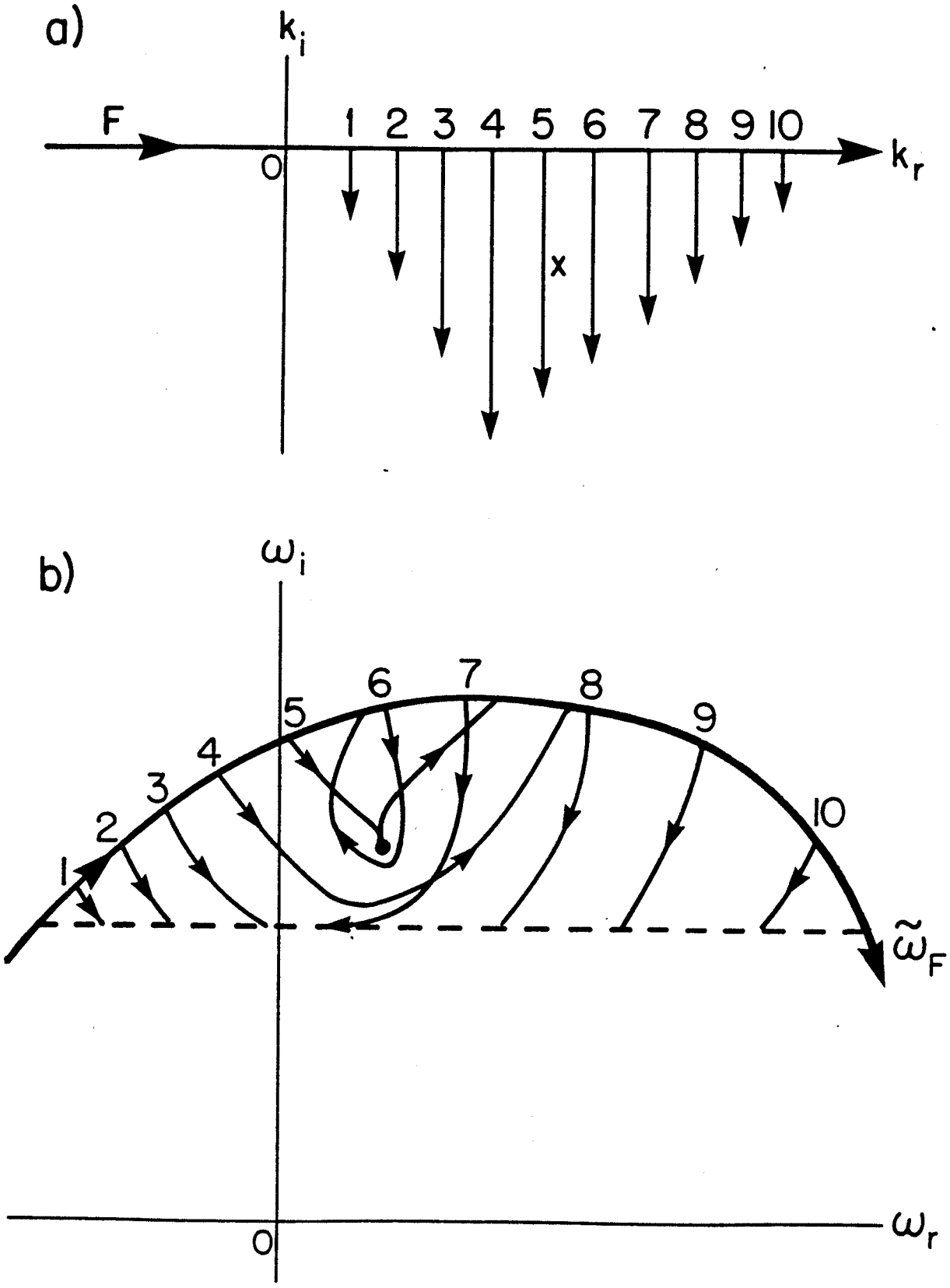
a)
k_i
F
1 2 3 4 5 6 7 8 9 10
0
k_r
x
b)
ω_i
1
2
3
4
5
6
7
8
9
10
$\tilde{\omega}_F$
0
ω_r

Figure 6 a, b

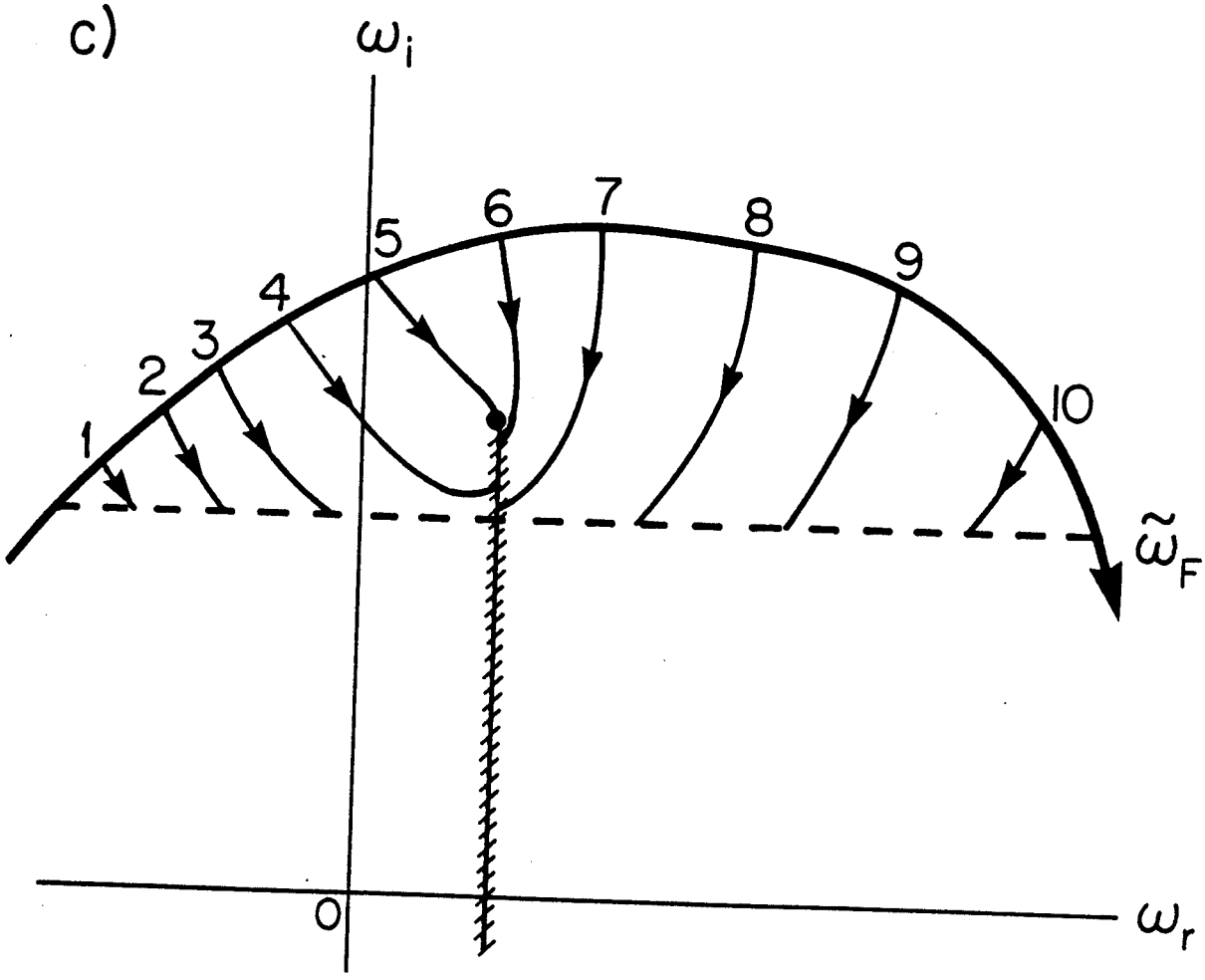

Figure 6c

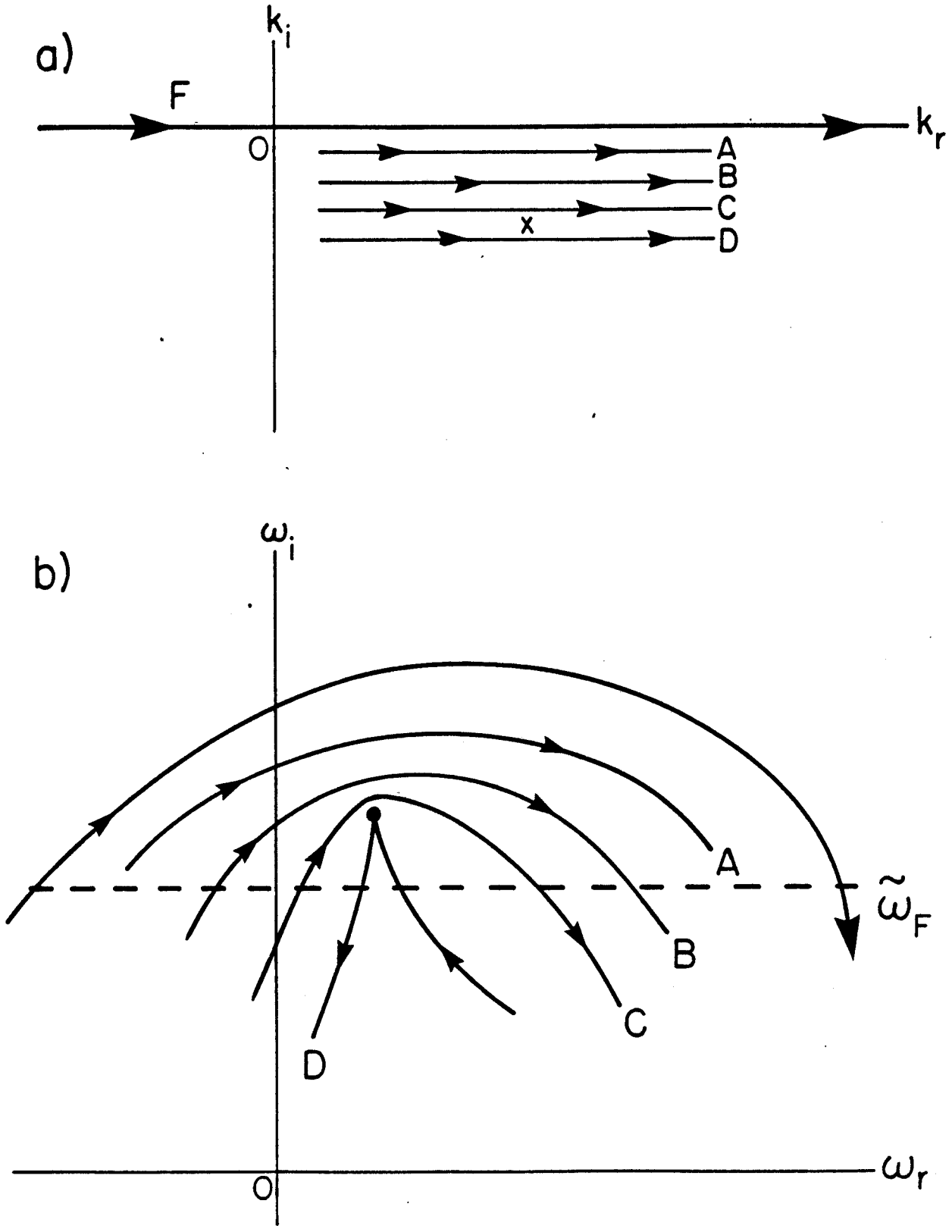

Figure 7 a, b

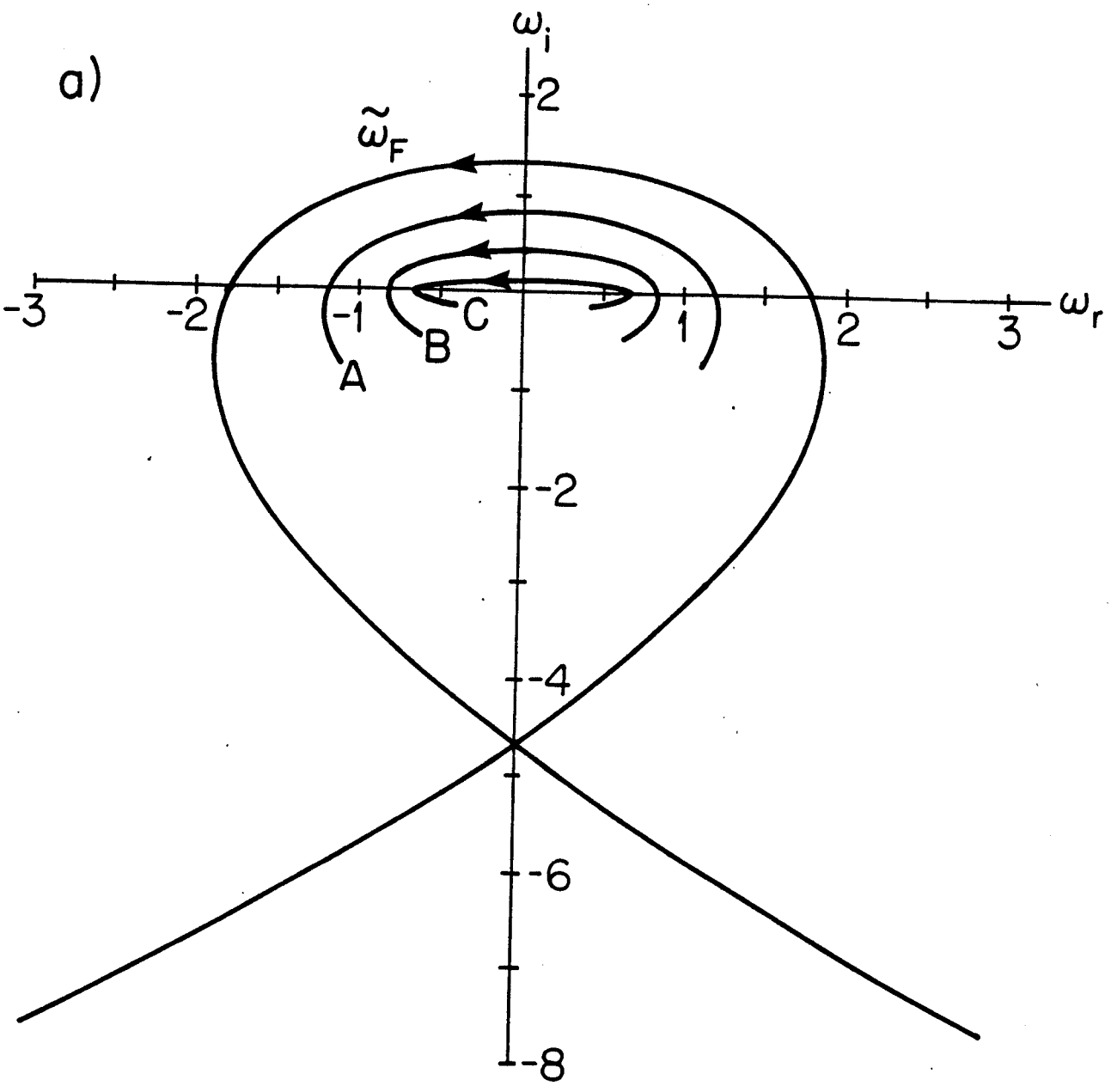

Figure 8 a

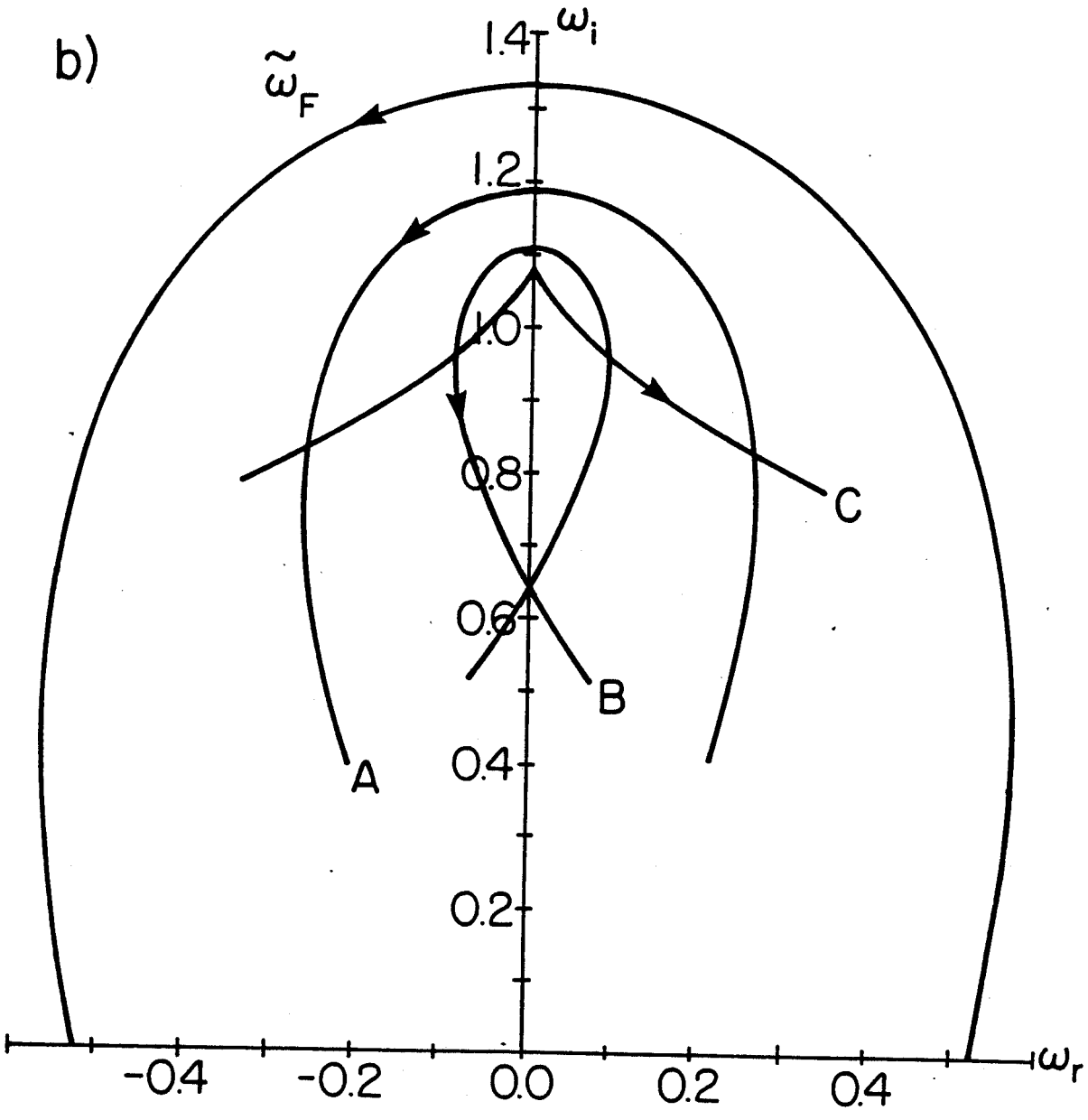
b)
$\tilde{\omega}_F$
ω_i
1.4
1.2
1.0
0.8
0.6
0.4
0.2
A
B
C
-0.4
-0.2
0.0
0.2
0.4
ω_r

Figure 8 b

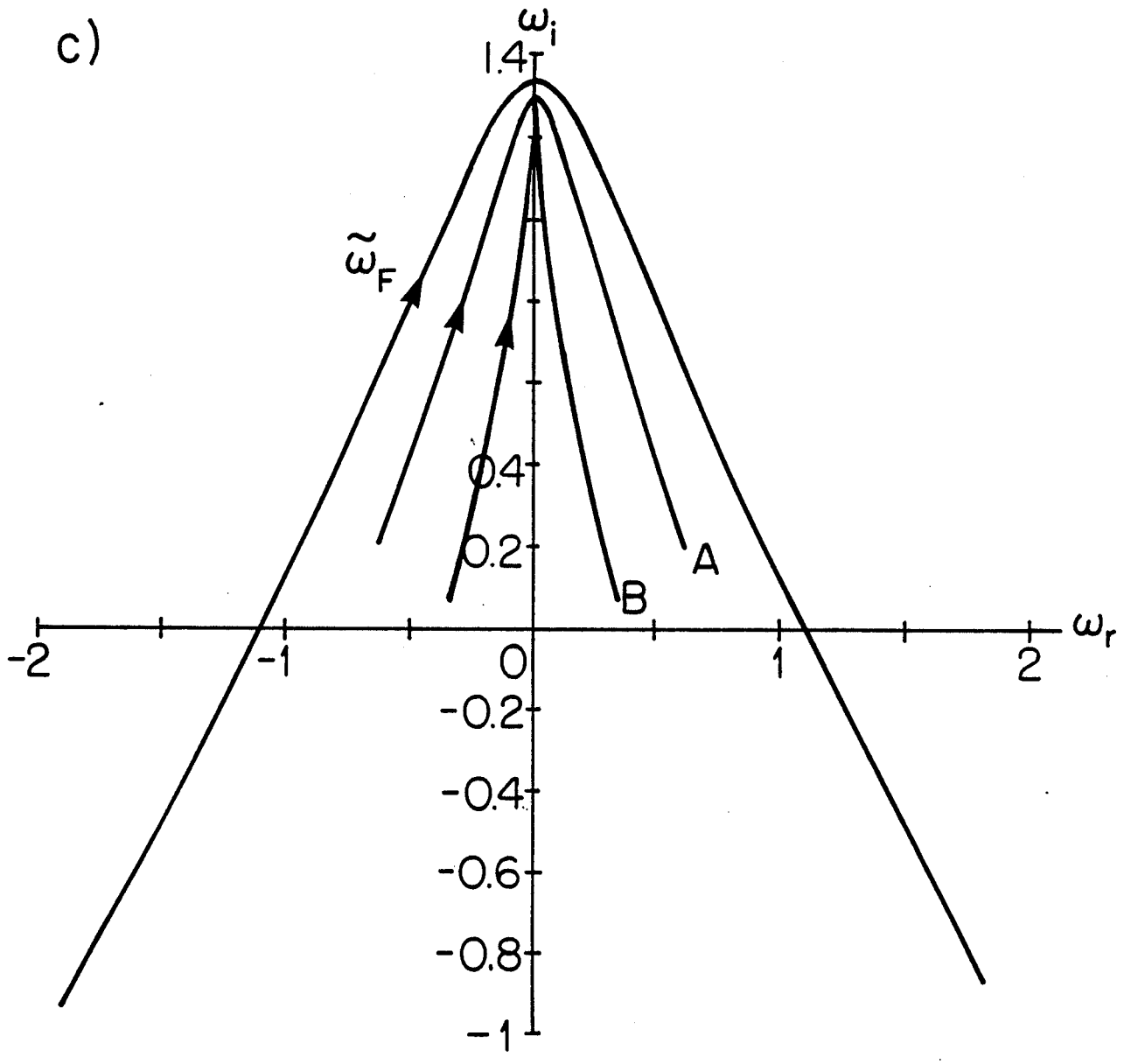

Figure 8 c

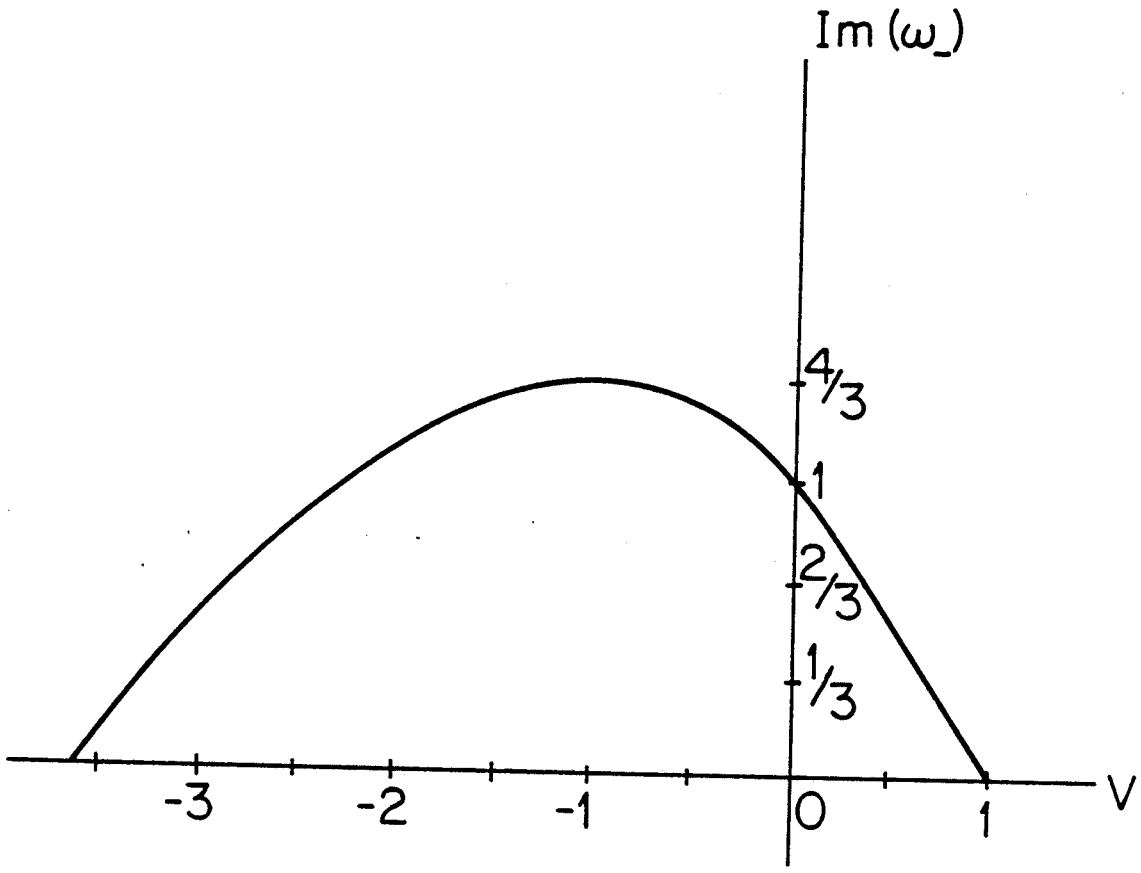

Figure 9

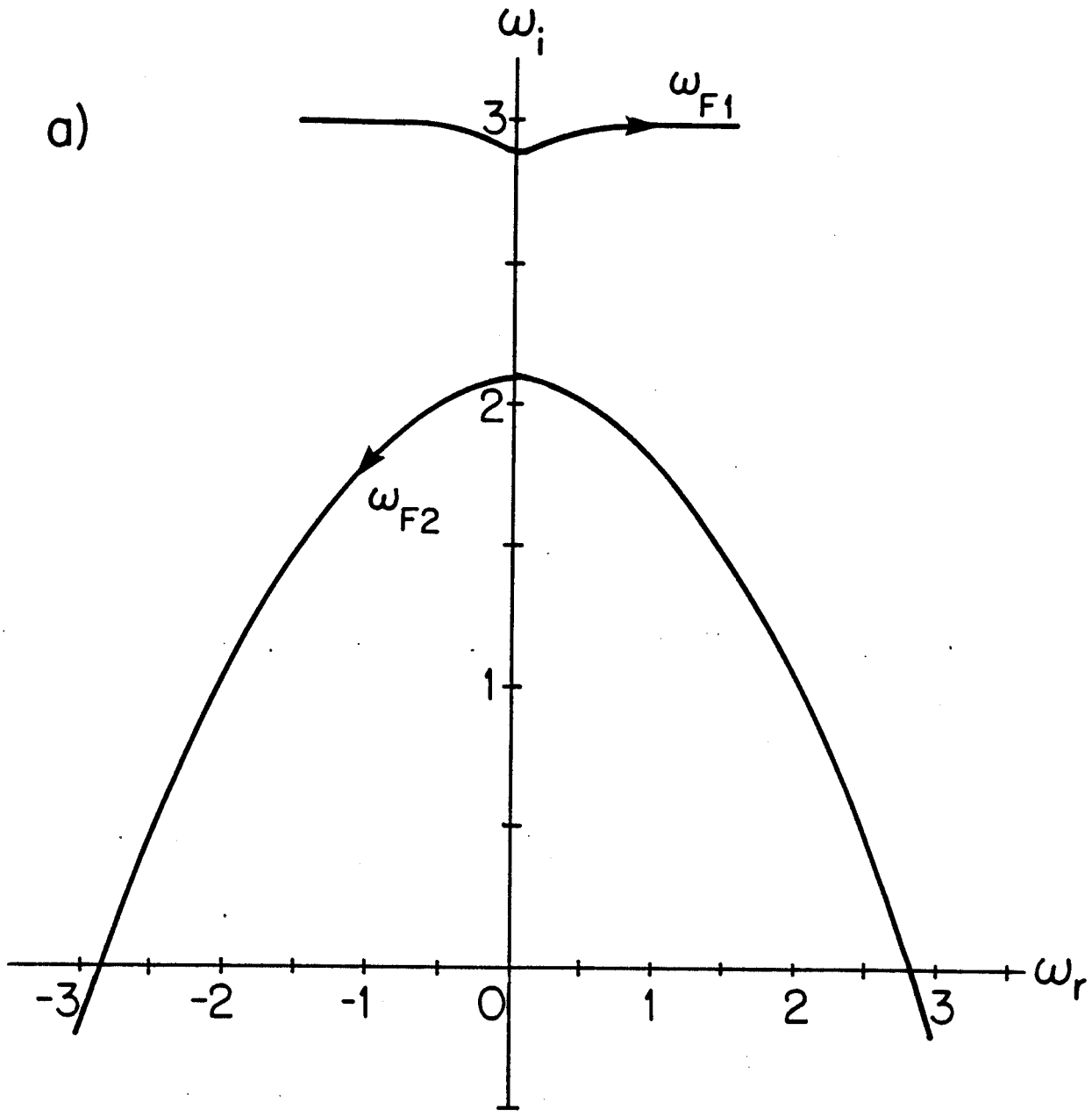

Figure 10 a

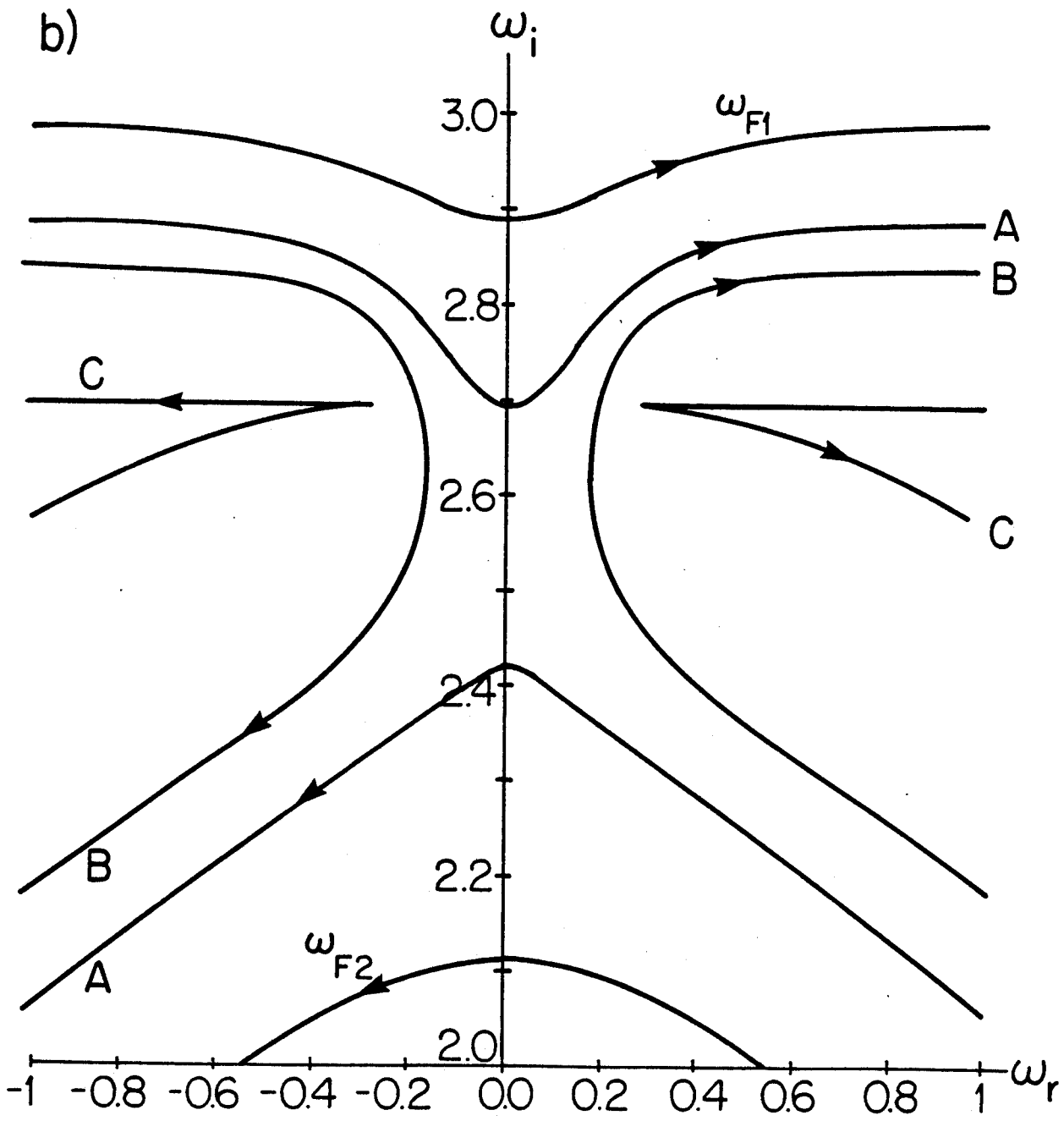
b)
ω_i
3.0
2.8
2.6
2.4
2.2
2.0
ω_{F1}
A
B
C
C
B
A
ω_{F2}
-1
-0.8
-0.6
-0.4
-0.2
0.0
0.2
0.4
0.6
0.8
1
ω_r

Figure 10 b

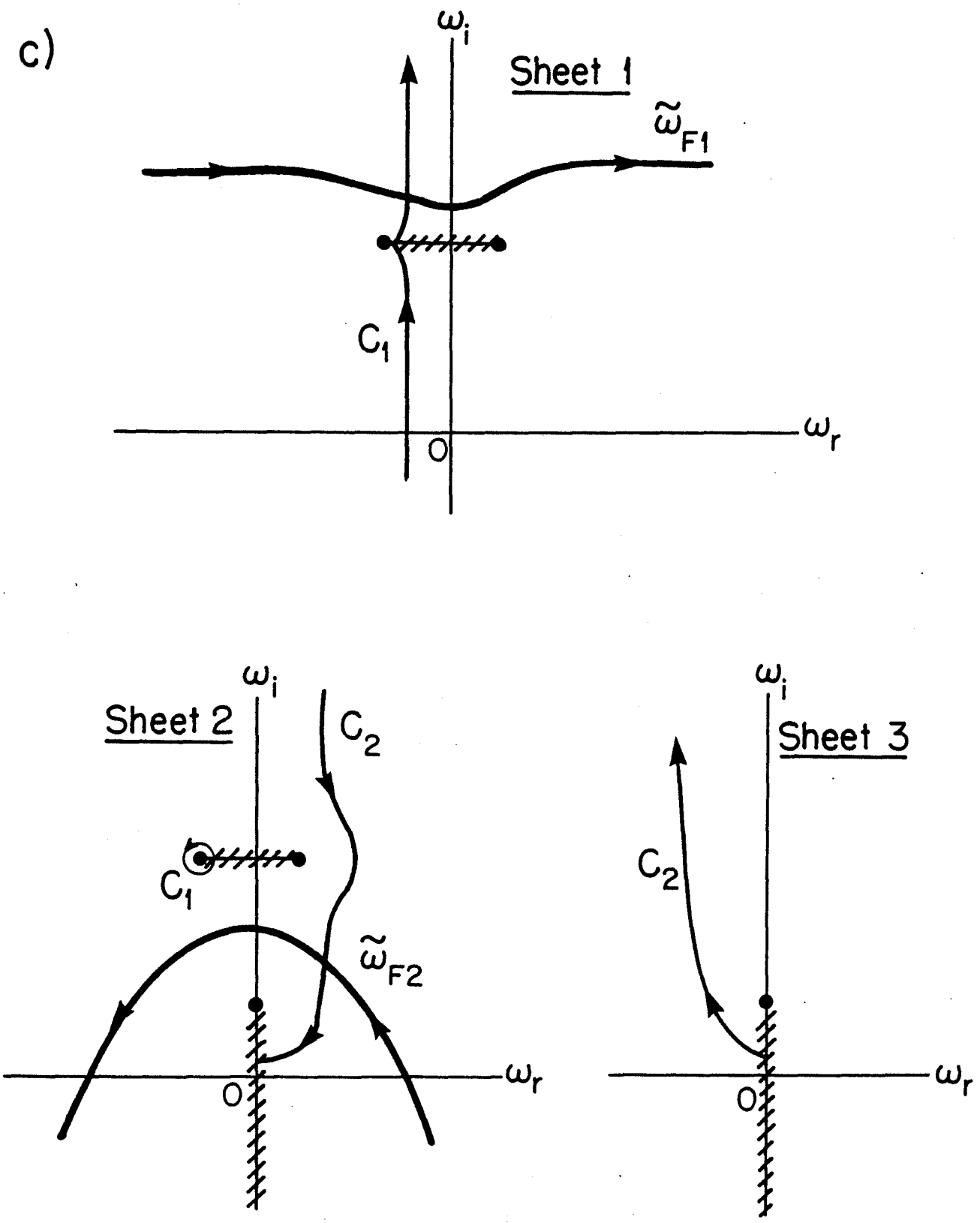
c)
ω_i
Sheet 1
$\tilde{\omega}_{F1}$
C_1
O
ω_r
ω_i
Sheet 2
C_2
C_1
$\tilde{\omega}_{F2}$
O
ω_r
ω_i
Sheet 3
C_2
O
ω_r

Figure 10c

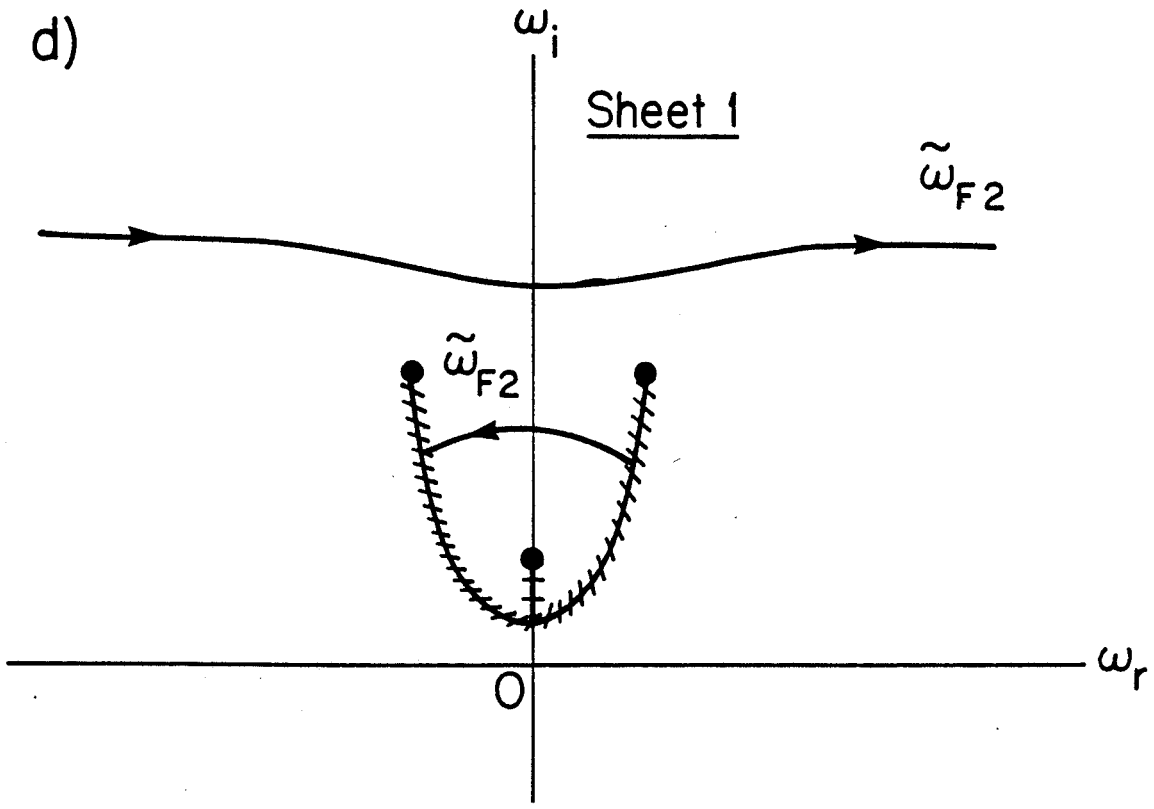

Figure 10d

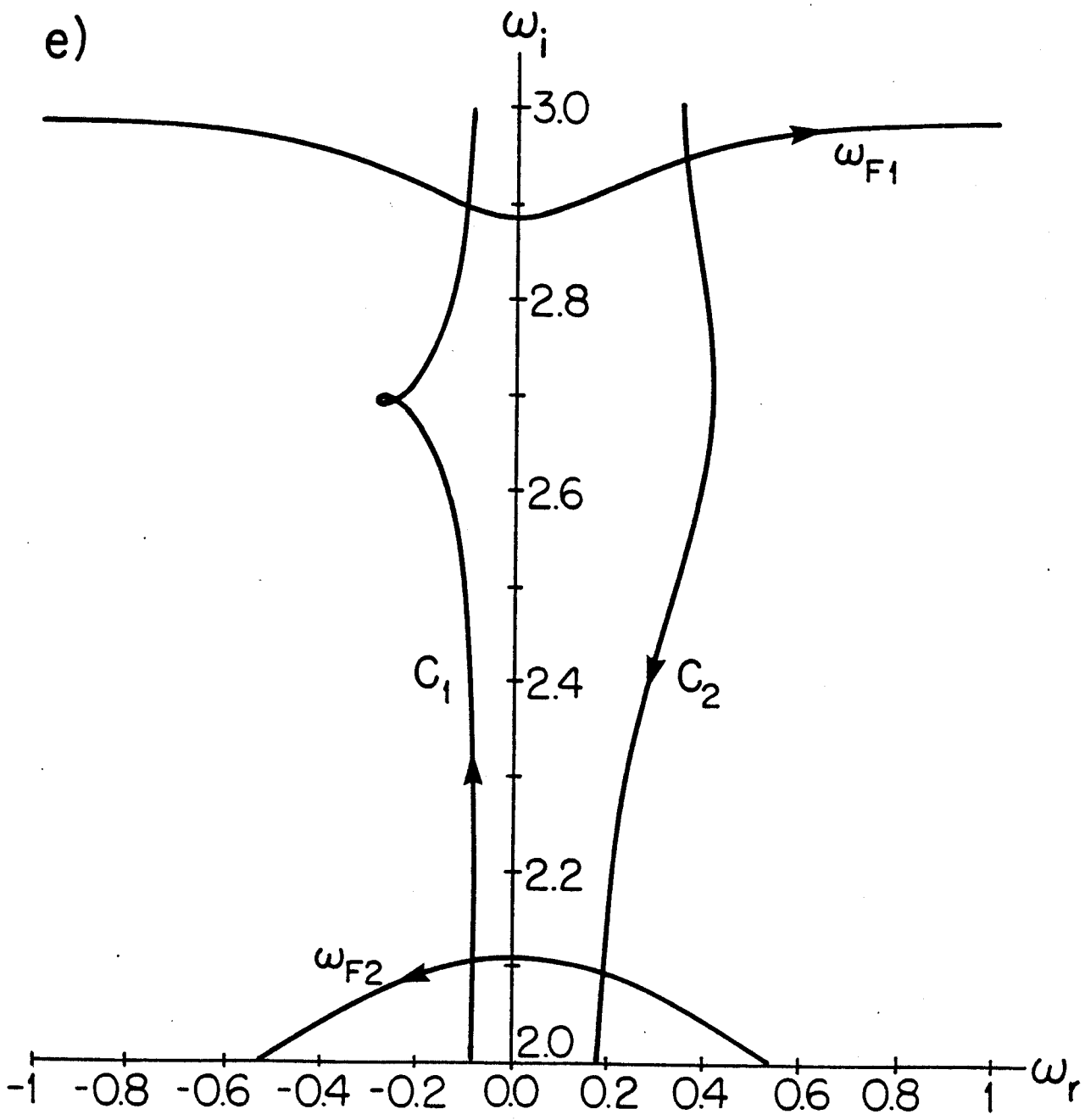
e)
ω_i
3.0
2.8
2.6
2.4
2.2
2.0
ω_{F1}
ω_{F2}
C_1
C_2
-1
-0.8
-0.6
-0.4
-0.2
0.0
0.2
0.4
0.6
0.8
1
ω_r

Figure 10e

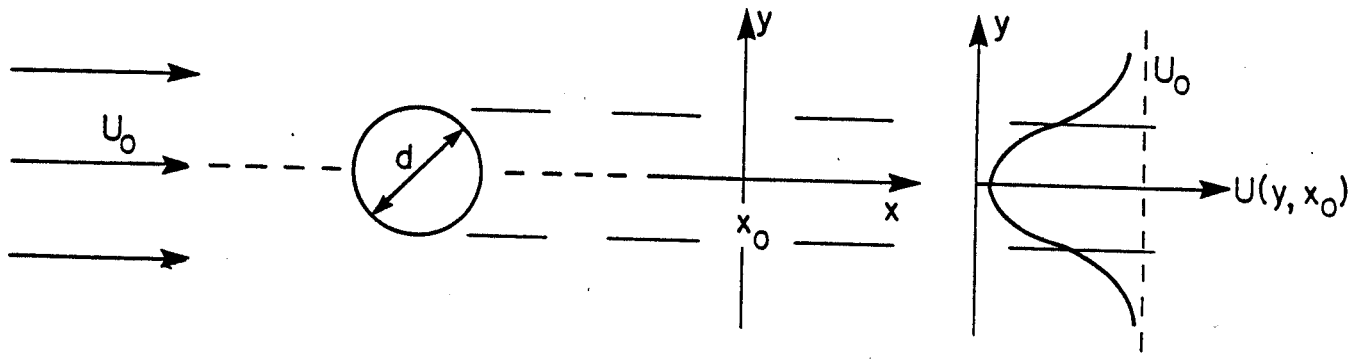

Figure 11

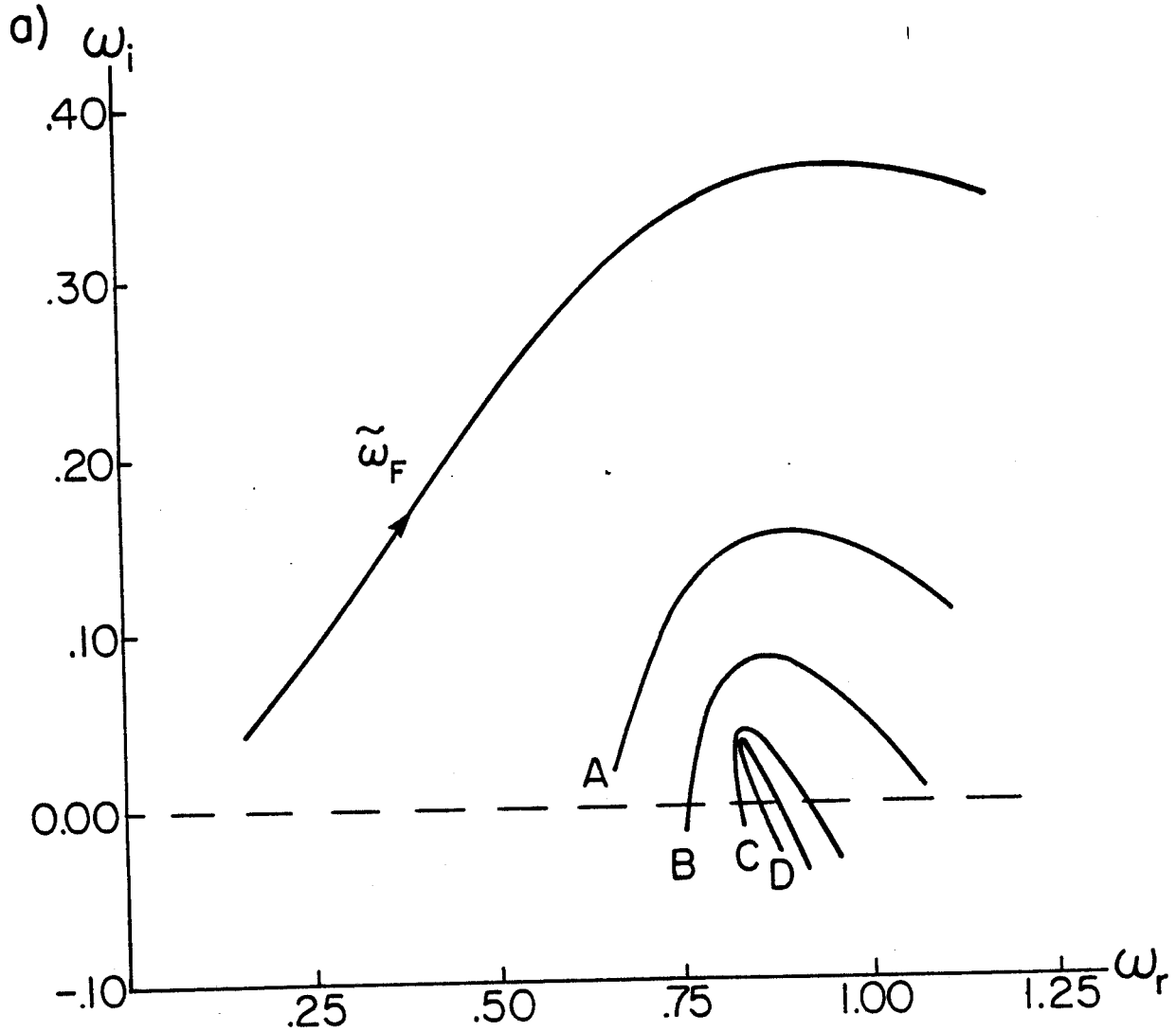
a) ω_i
.40
.30
.20
.10
0.00
-.10
$\tilde{\omega}_F$
A
B
C
D
.25
.50
.75
1.00
1.25
ω_r

Figure 12a

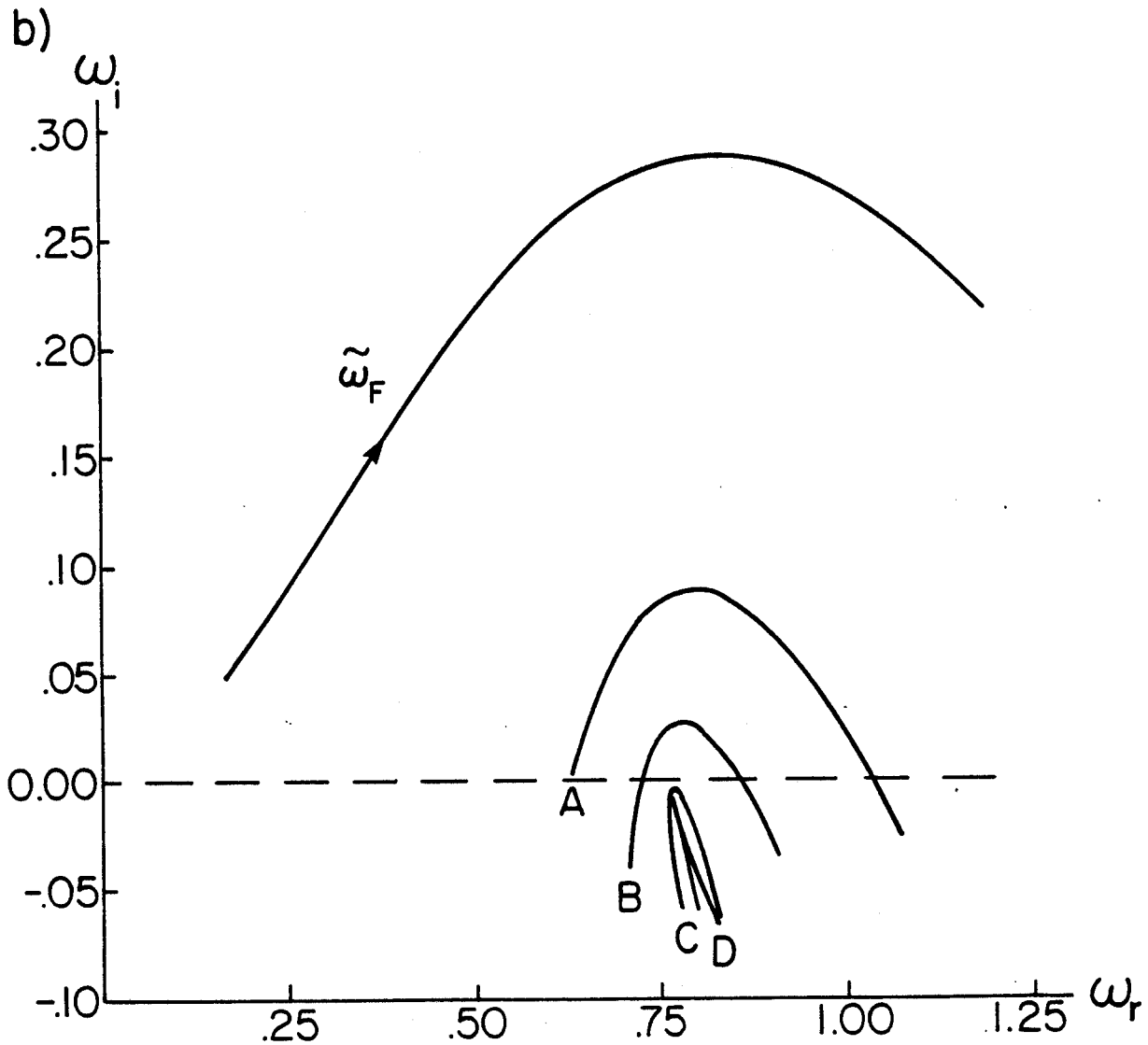
b)
ω_i
.30
.25
.20
.15
.10
.05
0.00
-.05
-.10
$\tilde{\omega}_F$
A
B
C
D
.25
.50
.75
1.00
1.25
ω_r

Figure 12b